J Therm Anal Calorim (2009) 98:707–716
DOI 10.1007/s10973-009-0287-x

Phase transformations of ammonium tungsten bronzes

Imre Miklós Szilágyi · István Sajó · Péter Király · Gábor Tárkányi · Attila L. Tóth · András Szabó · Katalin Varga-Josepovits · János Madarász · György Pokol

Received: 20 December 2008 / Accepted: 27 January 2009 / Published online: 12 August 2009

Abstract This article discusses the formation and structure of ammonium tungsten bronzes, $(NH_4)_xWO_{3-y}$. As analytical tools, TG/DTA-MS, XRD, SEM, Raman, XPS, and ^{1}H-MAS NMR were used. The well-known α-hexagonal ammonium tungsten bronze (α-HATB, ICDD 42-0452) was thermally reduced and around 550 °C a hexagonal ammonium tungsten bronze formed, whose structure was similar to α-HATB, but the hexagonal channels were almost completely empty; thus, this phase was called reduced hexagonal (h-) WO_3. In contrast with earlier considerations, it was found that the oxidation state of W atoms influenced at least as much the cell parameters of α-HATB and h-WO_3, as the packing of the hexagonal channels. Between 600 and 650 °C reduced h-WO_3 transformed into another ammonium tungsten bronze, whose structure was disputed in the literature. It was found that the structure of this phase—called β-HATB, $(NH_4)_{0.001}WO_{2.79}$—was hexagonal.

Keywords Ammonium tungsten bronze · Annealing · Phase transformations · Crystal structure · TG/DTA-MS · XRD · XPS · Raman · ^{1}H-MAS NMR

I. M. Szilágyi (✉)
Materials Structure and Modeling Research Group of the Hungarian Academy of Sciences, Budapest University of Technology and Economics, Szt. Gellért tér 4, Budapest 1111, Hungary
e-mail: imre.szilagyi@mail.bme.hu

I. Sajó · P. Király · G. Tárkányi
Institute of Structural Chemistry, Chemical Research Center of the Hungarian Academy of Sciences, Pusztaszeri út 59-67, Budapest 1025, Hungary

A. L. Tóth
Research Institute for Technical Physics and Materials Science, Hungarian Academy of Sciences, Konkoly-Thege út 29-33, Budapest 1121, Hungary

A. Szabó
Department of Organic Chemistry and Technology, Budapest University of Technology and Economics, Budafoki út 8, Budapest 1111, Hungary

K. Varga-Josepovits
Department of Atomic Physics, Budapest University of Technology and Economics, Budafoki út 8, Budapest 1111, Hungary

J. Madarász · G. Pokol
Department of Inorganic and Analytical Chemistry, Budapest University of Technology and Economics, Szt. Gellért tér 4, Budapest 1111, Hungary

Introduction

Tungsten oxides and tungsten bronzes have attracted much attention in the past decades owing to their promising physical and chemical properties. They are used as catalysts [1–3], they are potential candidates for electrochemical cells (e.g. fuel cells, secondary batteries, photoelectrochemical cells) [4–6], they are the most researched materials for chromogenic (electro- [7–10], photo- [11, 12], gaso- [13], and thermochromic [14, 15]) devices, and their application as gas sensors to various gases (NH_3, NO_2, H_2S, etc.) is also remarkable [16–19].

Ammonium tungsten bronzes, $(NH_4)_xWO_{3-y}$ are particularly interesting members of tungsten oxides and tungsten bronzes. Traditionally they are important intermediates in the powder metallurgical production of tungsten powder for lamp and hard metal industry [20, 21]. In addition they have open-tunnel structure, they can exchange their NH_4^+ ions with metallic cations [22–25],

and they have mixed conductivity, i.e., they can conduct both protons (because of H^+ containing species such as NH_3, NH_4^+, H_2O, OH-group) and electrons (because of electron hopping between W^{6+}, W^{5+} and W^{4+} atoms) [26]. These unique features make ammonium tungsten bronzes promising compounds for the several, previously mentioned application fields.

The most important ammonium tungsten bronze is α-hexagonal ammonium tungsten bronze (α-HATB, ICDD 42-0452). It can be prepared also by hydrothermal [26, 27] and solvothermal [28, 29] synthesis methods, but the partial reduction of ammonium paratungstate (APT), $(NH_4)_{10}[H_2W_{12}O_{42}]\cdot 4H_2O$ between 300 and 500 °C is the best way to produce it in a highly crystalline form [30–32]. The structure of α-HATB is built up by corner sharing octahedra, which form three- and six-sided channels along the structure [20]. NH_4^+ ions (and NH_3 molecules as well) occupy the cavities in the hexagonal channels. If the channels are completely filled, then $x = 0.33$ in $(NH_4)_xWO_{3-y}$.

The second type of ammonium tungsten bronzes is formed, if α-HATB is annealed between 400 and 550 °C [33]. The product is called in the literature hexagonal tungsten oxide (h-WO_3, ICDD 85-2460), though this nomination is somewhat misleading. The structure of α-HATB and h-WO_3 are practically the same, the only difference is that in h-WO_3 the hexagonal channels are considered to be empty. However, it was shown recently, that in general the structure of h-WO_3 cannot be maintained without some stabilizing ions or molecules in the hexagonal channels [33], which means that the hexagonal channels of h-WO_3 are not completely empty. Therefore, the strictly stoichiometric h-WO_3 does not exist, it is just an idealized compound, and all h-WO_3 samples are in fact hexagonal tungsten bronzes with very low residual ion or molecule content. It follows that the h-WO_3 produced from α-HATB is in real a hexagonal ammonium tungsten bronze with the same structure as α-HATB but with a very low NH_4^+ and NH_3 content.

There is a third type of ammonium tungsten bronzes that has been reported in the literature. This phase appeared during the thermal reduction of ammonium paratungstate (APT), $(NH_4)_{10}[H_2W_{12}O_{42}]\cdot 4H_2O$ [30, 34], ammonium tungstate, $(NH_4)_2WO_4$ [35], or α-HATB [36, 37] between 550 and 700 °C. There is not agreement about its structure, which is indicated by that two different ICDD cards have been assigned to it. One of the cards describes a tetragonal ammonium tungsten bronze, $(NH_4)_{0.06}WO_3(H_2O)_{0.11}$ (ICDD 15-0217), while the other one reports a hexagonal ammonium tungsten bronze, $(NH_4)_{0.42}WO_3$ (ICDD 42-0451).

Since ammonium tungsten bronzes have both scientific and industrial significance, we intended to clear the picture about their formation, structure and phase transition. Recently we have already studied the formation of α-HATB and proposed an explanation how monophase α-HATB could be produced [31]. Based on this we managed to prepare monophase, nanosize α-HATB, whose structure and composition were analysed thoroughly [31]. Since the other two kinds of ammonium tungsten bronzes are believed to appear during the thermal reduction of α-HATB, having a high quality α-HATB precursor allowed us to study the formation, structure and composition of the two other ammonium tungsten bronzes. This study was also encouraged by that there was only one previous report [24] about the thermal reduction of α-HATB, but it did not contain structure or composition analyses.

Therefore, we studied the thermal reduction of α-HATB in 10% H_2/He and 10% H_2/Ar with simultaneous TG/DTA and on-line coupled evolved gas analysis (TG/DTA-MS) up to 900 °C to gain a general insight about the thermal processes involved. Intermediate solid products were analyzed by powder X-ray diffraction (XRD). As a result we observed the formation of the two other kinds of ammonium tungsten bronzes from α-HATB. To get a detailed view on their composition and morphology, we used X-ray photoelectron spectroscopy (XPS), Raman spectroscopy, solid state ^{1}H-MAS (magic angle spinning) NMR spectroscopy and scanning electron microscopy (SEM). Finally as we could obtain the ammonium tungsten bronze, which had two different ICDD cards (ICDD 15-0217 and 42-0451), in a pure form, it could be decided whether this phase had hexagonal or tetragonal structure: it was concluded that it had hexagonal.

Experimental section

Monophase, nanosize α-hexagonal ammonium tungsten bronze, α-HATB, $(NH_4)_{0.08}(NH_3)_{0.04}(H_2O)_{0.09}WO_{2.93}$ was prepared by heating ammonium paratungstate tetrahydrate (APT), $(NH_4)_{10}[H_2W_{12}O_{42}]\cdot 4H_2O$ in H_2 for 6 h at 400 °C [31]. Table 1 comprises the experimental conditions (decomposition atmosphere and temperature) for selected samples prepared from α-HATB.

The evolved gas analytical (TG/DTA-MS) apparatus consisted of an STD 2960 Simultaneous DTA/TGA (TA Instruments Inc.) thermal analyzer and a Thermostar GSD 200 (Balzers Instruments) quadrupole mass spectrometer. The details of the TG/DTA-MS setup are discussed elsewhere [30, 38].

XRD patterns of decomposition intermediates of α-HATB were recorded by a PANalytical X'pert Pro MPD X-ray diffractometer equipped with an X'Celerator detector using CuK_α radiation. For lattice parameter determination of β-hexagonal ammonium tungsten bronze (β-HATB) a Philips PW-1830 X-ray diffractometer was

Table 1 W oxidations states*, amount of NH_4^+ and NH_3 compared to W atoms (x in $(NH4)_xWO_{3-y}$), cell parameters and selected d values for α-HATB, various h-WO_3 samples and β-HATB

Samples (with annealing conditions of α-HATB)	W^{6+}/%	W^{5+}/%	W^{4+}%	W (average oxidation number)	$NH_4^+ + NH_3$/W	a/nm	c/nm	V_0/nm^3	d_{200}/nm	d_{002}/nm	d_{202}/nm	d_{112}/nm
α-HATB	82.3	12.9	4.8	5.78	0.12	0.7380	0.7542	0.3557	0.3196	0.3771	0.2438	0.2637
Reduced h-WO_3 (10% H_2/Ar, 550 °C	77.3	15.9	6.8	5.71	0.011	0.7395	0.7586	0.3593	0.3202	0.3793	0.2447	0.2648
h-WO_3 (N_2, 550 °C)	88.1	7.9	4.0	5.84	0.010	0.7370	0.7612	0.3580	0.3191	0.3806	0.2445	0.2647
h-WO_3 (air, 400 °C)	94.6	3.9	1.5	5.93	0.025	0.7341	0.7645	0.3568	0.3179	0.3823	0.2444	0.2647
h-WO_3 (air, 470 °C)	96.8	1.8	1.4	5.95	0.019	0.7341	0.7662	0.3575	0.3179	0.3831	0.2446	0.2650
β-HATB (10% H_2/Ar, 650 °C)	69.9	17.6	12.5	5.57	0.002	0.7305	0.7568	0.3498				

* $W4f_{7/2}$ peaks (37.1, 36.0, 34.7 eV for W^{6+}, W^{5+}, W^{4+}, respectively); $W4f_{5/2}$ peaks (35.0, 33.7, 32.8 eV for W^{6+}, W^{5+}, W^{4+}, respectively)

used. Corundum, Al_2O_3 (NIST SRM 676, 0.475919 nm/1.299183 nm, ICDD 43-1284) was applied as a line position standard reference material. Peak positions and intensities were determined with a full profile fit after CuK_{α_2} strip.

XPS spectra were collected by a VG Microtech instrument consisting of a XR3E2 X-ray source, a twin anode (MgK_α and AlK_α) and a CLAM 2 hemispherical analyser using MgK_α radiation. Detailed scans were recorded with 50 eV pass energy at (0.05 eV/1.5 s). The spectrometer was calibrated with the binding energy of the C 1s line (284.5 eV).

Raman spectra were collected by a Jobin Yvon Labram instrument attached to an Olympus BX41 microscope. Frequency doubled Nd–YAG laser (532 nm) was applied as exiting source with 1 mW applied power. The sample was located and examined with a 50× objective, thus individual crystals could be examined (laser spot size was about 1.2 μm). The backscattered light collected by the objective was dispersed on an 1800 g/mm grating and detected by a 1024 × 256 CCD detector.

^{1}H-MAS NMR experiments were carried out on a VARIAN NMR SYSTEM spectrometer (600 MHz for ^{1}H) using a 3.2 mm HXY VARIAN/Chemagnetics probe. ^{1}H chemical shifts were referenced to adamantane ($\delta_{1H} = 0$ ppm). All spectra were recorded under the same experimental conditions. Recycle delays were optimized by arrayed experiments and proton pulse widths were calibrated for each sample to achieve comparability and to allow quantitation of the components. Sixteen transients were acquired at 12 kHz spinning rate and a recycle delay of 20 s was used. Background suppression DEPTH [39] was employed to remove signals from the probe.

SEM characterization was performed by a LEO-1550 FEG SEM instrument.

Results and discussion

Formation of reduced h-WO_3

The simultaneous TG, DTG, DTA curves of the thermal reduction of α-HATB are presented in Fig. 1. Seven decomposition steps were observed up to 900 °C, which are marked on the DTG curve. With evolved gas analysis the evolution of H_2O and NH_3 was detected (Fig. 1). X-ray patterns of decomposition intermediates of α-HATB are shown in Fig. 2.

Up to 250 °C absorbed and chemisorbed H_2O evolved in two overlapping endothermic reactions (DTG curve, peaks 1–2). From 250 to 650 °C water and ammonia were released in three overlapping steps (DTG curve, peaks 3–5, 250–450, 450–500, 500–650 °C). The release of NH_3

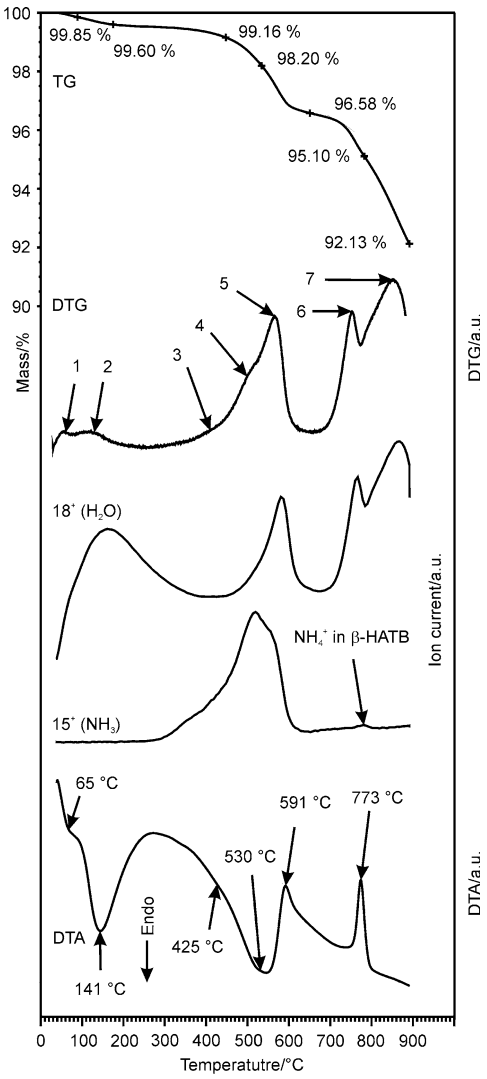

Fig. 1 Simultaneous TG/DTG/DTA and evolved gas analytical (MS ion) curves of α-HATB measured in 10% H_2/He (130 mL min^{-1}, 10 °C min^{-1}, open Pt crucible, 150.9 mg)

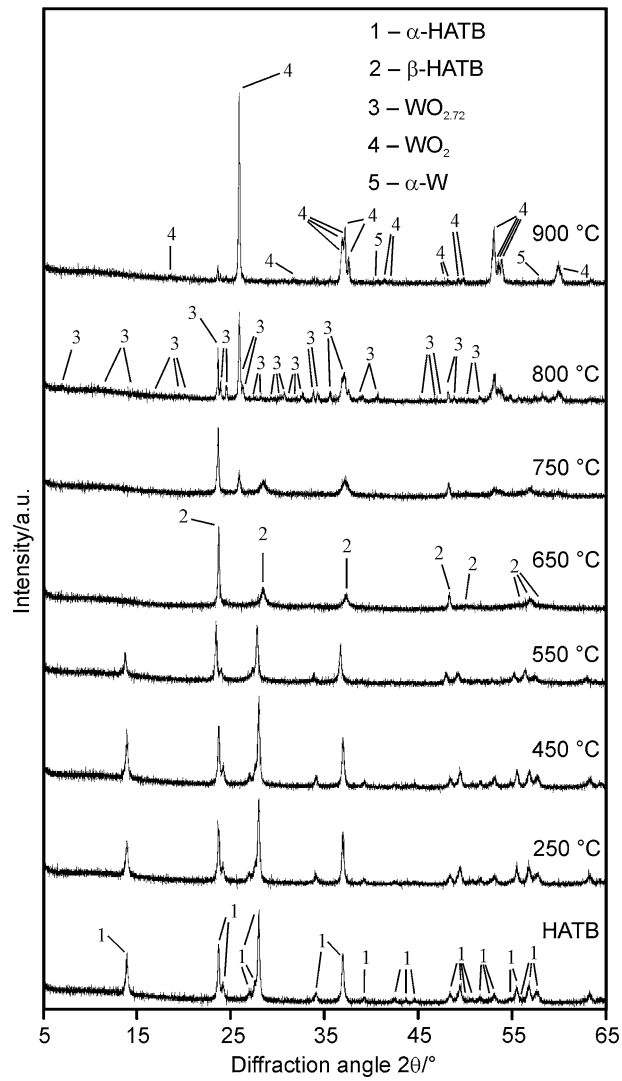

Fig. 2 XRD patterns of intermediate solid products of α-HATB decomposed in 10% H_2/Ar

below 400 °C was unexpected, because α-HATB was produced by heating APT at 400 °C in H_2 [31]. This early evolution of NH_3 can be explained either by cracking of α-HATB samples after their preparation at 400 °C, which produced new open particle surfaces filled partly with NH_3 and NH_4^+. The other explanation is that in a solid state chemical equilibrium reaction rearrangement of NH_4^+ ions and NH_3 molecules could have occurred in as-prepared α-HATB, and due to this from the bulk some part of NH_3 and NH_4^+ could have moved onto the surface of α-HATB particles, from where they could be released below 400 °C.

The release of NH_3 molecules in three consecutive steps was explained by that NH_3 molecules (which originated from the NH_4^+ and NH_3 content of α-HATB [22, 23, 31]) came from three different positions of α-HATB particles, where they were bonded with different strength. In the first step they came from the surface of the particles, in the second step either from a second surface position or from the disordered space between the crystallite and in the third step from the hexagonal channels of the crystallites. We discussed recently the detection of different cation positions in α-HATB in detail [33]. More explanations were considered for the origin of NH_3, which evolved in three different steps, and on the basis of theoretical considerations and experimental results, the explanation above was found to be the most probable.

Despite the continuous release of NH_3 and H_2O, the structure of α-HATB (ICDD 42-0452) did not change. At 450 °C the XRD pattern was almost the same as at room temperature, and by 550 °C only the crystalline order of the sample decreased slightly. The major difference between α-HATB and the decomposition intermediate at 550 °C was that the hexagonal channels became almost

completely empty at 550 °C (shown indirectly by TG/DTA-MS, and also directly by ^{1}H-MAS NMR as discussed later). Therefore, to indicate this change and to be consistent with the literature, this phase was called reduced h-WO_3.

Characterization of reduced h-WO_3

As revealed by XPS, already α-HATB was partly reduced, as it contained W^{4+} and W^{5+} atoms besides W^{6+} atoms (Fig. 3; Table 1). After annealing in reducing atmosphere at 550 °C, the ratio of reduced tungsten atoms increased in the product reduced h-WO_3. The reduced state of α-HATB and reduced h-WO_3 was also supported by their dark blue colour.

Raman spectra showed that the bands of α-HATB were quite broad due to the partly reduced state of W atoms (Fig. 4). Therefore, it was difficult to assign the bands to certain vibrations, particularly the broad peak below 500 cm^{-1}, which might be deconvoluted into several deformation and lattice vibrations. The main band at 721 cm^{-1} and the shoulder at 654 cm^{-1} can be assigned to stretching O–W–O modes, but other overlapping peaks may be also present. The small peak at 988 cm^{-1} should be attributed to stretching mode of the terminal W=O [40]. Though this latter band is characteristic to tungsten oxide hydrates, this can also appear in α-HATB, because this compound adsorbs relatively high amount of H_2O molecules [41] due to its active ionic surface [22]. In reduced h-WO_3, as the ratio of reduced tungsten atoms increased, the Raman peaks became more diffuse.

We measured the amount of NH_4^+ ions and NH_3 molecules, which remained in the solid structure, by solid-state ^{1}H NMR spectroscopy (Fig. 5) [22, 23, 31]. After curve fitting the ^{1}H-MAS NMR spectrum of α-HATB, the peaks at 4.5 and 5.6 ppm were assigned to NH_4^+ ions and NH_3 molecules, respectively. This assignment relies on the assumption that the peak positions do not interchange upon morphological changes. The ^{1}H-MAS NMR results showed that due to annealing the amount of NH_4^+ ions and NH_3 molecules decreased, but they were still present in reduced h-WO_3.

According to SEM analysis, the precursor of α-HATB, i.e., ammonium paratungstate tetrahydrate (APT), $(NH_4)_{10}[H_2W_{12}O_{42}]\cdot 4H_2O$ was polycrystalline and consisted of μm scale particles. When α-HATB was produced from APT, the micro-morphology was preserved (Fig. 6a), but the nano-morphology changed a great deal, because 50–100 nm α-HATB particles were formed as α-HATB was crystallizing (Fig. 6b). The annealing of α-HATB did not affect the morphology of the nanoparticles, and reduced h-WO_3 was also built up by aggregated 50–100 nm particles (Fig. 6c).

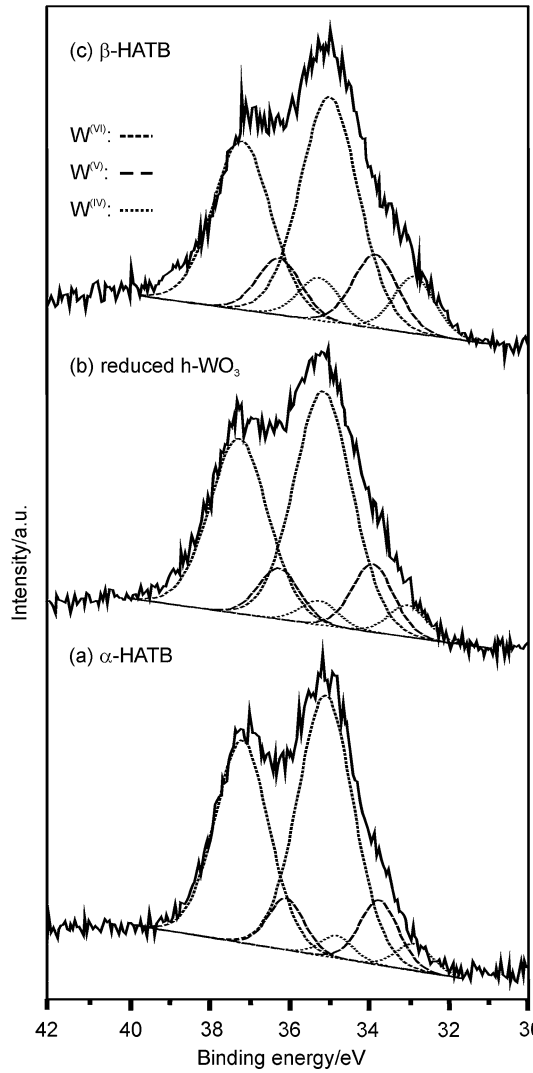

Fig. 3 XPS spectra (W4f region) of: **a** α-HATB; **b** reduced h-WO_3 and **c** *β*-HATB

By analysing the XRD data and the composition of α-HATB and of various h-WO_3 samples, we concluded that the oxidation state of W atoms influenced at least as much the cell parameters of the samples, as the occupancy of the hexagonal channels. This is significant, since previously only packing of the hexagonal channels was considered to be decisive on the cell parameters of h-WO_3 and α-HATB (and in general also on the cell parameters of hexagonal tungsten bronzes) [21]. Besides reducing α-HATB in 10% H_2/Ar (reduced h-WO_3 sample), h-WO_3 samples with different oxidation states were prepared by annealing α-HATB in air and N_2. In Table 1 the average oxidation number of W atoms shows the general reduced/oxidized state of the samples, while the overall amount of NH_4^+ and NH_3 gives the occupancy of the hexagonal channels. Only the sum of NH_4^+ and NH_3 is shown, since on the one hand to estimate the packing of the hexagonal channels both

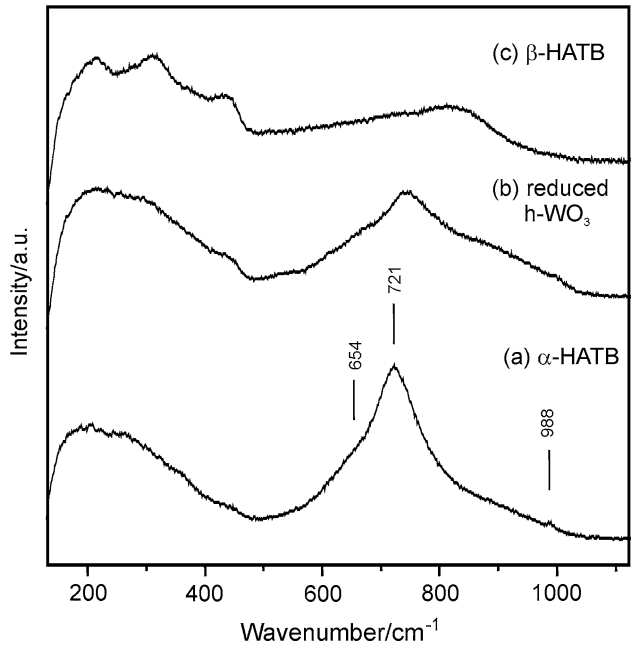

Fig. 4 Raman spectra of: (a) α-HATB; (b) reduced h-WO_3 and (c) *β*-HATB

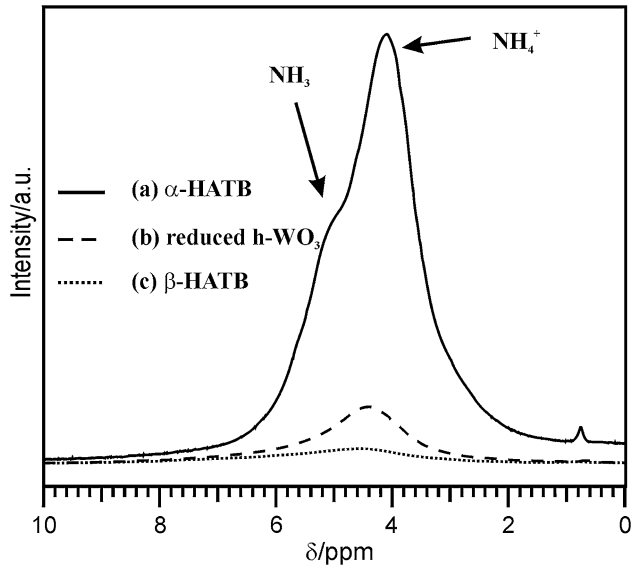

Fig. 5 ^{1}H-MAS NMR spectra of: (a) α-HATB; (b) reduced h-WO_3 and (c) *β*-HATB

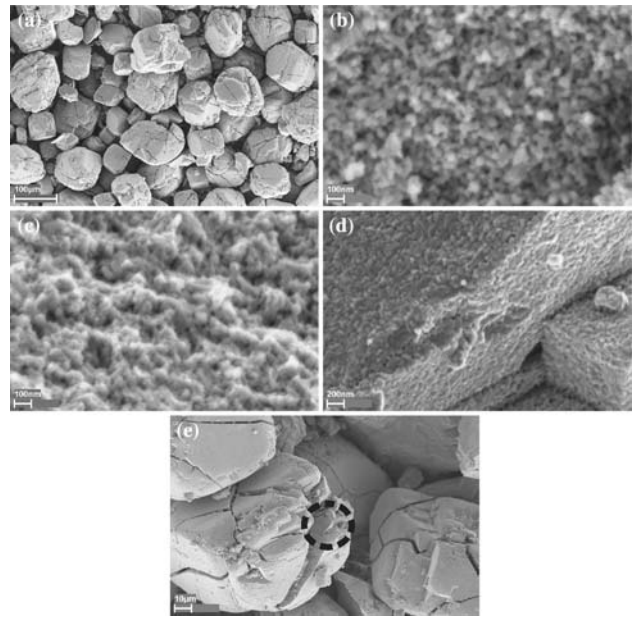

Fig. 6 SEM images of: **a** micromorphology of α-HATB; **b** nanograins of α-HATB; **c** nanograins of reduced h-WO_3 and **d** nanograins of *β*-HATB; **e** micromorphology of *β*-HATB—the circle shows the region from where **d** was taken

NH_4^+ and NH_3 had to be taken into account, on the other hand it was difficult to deconvolute precisely the largely decreased peak at 5 ppm.

It can be clearly seen that as the packing of the hexagonal channels in h-WO_3 samples decreased compared to α-HATB, the *c* cell parameter increased, which is harmony with previous results [22]. This is explained by that as there were less ions or molecules in the channels, their electrostatic contracting effect also decreased, and the channels expanded along the *c* axis. However, the *c* cell parameter was also influenced by the oxidation state of W atoms. In case of reduced h-WO_3, the increase of *c* was significantly smaller then for h-WO_3 prepared in N_2, while the main difference between these two samples was their oxidation state, and not the packing of the hexagonal channels, which was nearly the same.

As a contrast, the *a* cell parameter was determined practically only by the oxidation state of W atoms. As W atoms became reduced in reduced h-WO_3, compared to α-HATB, the *a* cell parameter increased. However, as W atoms became more and more oxidized (h-WO_3 samples prepared in N_2 and air), the *a* cell parameter decreased.

As *a* and *c* changed mostly in an opposite direction, the volume of the unit cell showed smaller changes, but it was different for all samples. It is quite interesting that while the d_{200} and d_{002} reflections followed the change of *a* and *c* cell parameters in a self-understandable way, the d_{202} and d_{112} reflections remained nearly intact, though the composition changed a great deal. This is most striking in the case of d_{112} for α-HATB and for h-WO_3 samples prepared in 10% H_2/Ar (550 °C), N_2 (550 °C), and air (400 °C).

Formation of *β*-HATB

At the fifth DTG peak (500–650 °C) of the decomposition of α-HATB (Fig. 1), the evolution of NH_3 and H_2O started as an endothermic reaction (530 °C) similarly as at the

third and fourth DTG peaks, but soon changed into exothermic. The source of this exothermic heat effect at 590 °C could be explained by the help of XRD patterns. As α-HATB was heated, the structure remained practically the same. Then between 550 and 650 °C the hexagonal structure collapsed, when most of the stabilizing NH_3 molecules and NH_4^+ ions were purged out of reduced h-WO_3 (the stabilizing effect of these species is discussed elsewhere [33]). Since here the metastable h-WO_3 transformed into a more stable compound, this reaction was exothermic, and it changed the DTA curve into exothermic. Recently it was found that in oxidative and inert atmospheres the hexagonal WO_3 structure also collapsed in an exothermic reaction, but there h-WO_3 transformed into monoclinic (m-) WO_3 [33]. Here, in reductive atmosphere the hexagonal structure was highly reduced, and this oxygen lacking environment blocked the formation of m-WO_3. Instead, the ammonium tungsten bronze with disputed structure (ICDD 15-0217 and 42-0451) appeared in a pure form.

Characterization of β-HATB

The fact that we could prepare this phase in a pure form allowed us to decide, whether it had hexagonal or tetragonal structure. In order to obtain precise powder XRD data, corundum was used (NIST SRM 676, 0.475919 nm/1.299183 nm, ICDD 43-1284) as a line position standard reference material. Peak positions and intensities were determined with a full profile fit after CuK_{α_2} strip. The obtained reflections are listed in Table 2. Already, based on theoretical assumptions, Dickens et al. [42] thought that this ammonium tungsten bronze should not be tetragonal, since the inscribed spheres of available cavities were too small for ammonium ions in the tetragonal tungsten bronze structure. Now, we tried to index the measured reflections both in the tetragonal and the hexagonal systems. XRD patterns were fitted in both systems, and cell parameters were refined. We obtained a very good fit only for the hexagonal system. Therefore, analysis of XRD data clearly showed and gave experimental proof that the measured reflections could be indexed on a hexagonal cell and not on a tetragonal. As a result of XRD analysis, the following cell parameters were determined for β-HATB:

$$a = 0.7305 \pm 0.0002 \text{ nm}$$
$$c = 0.7568 \pm 0.0002 \text{ nm}.$$

The cell could be indexed with $c = 0.3784$ nm as well, but the double cell was chosen to ensure consistency with previous results.

In harmony with Volkov et al. [37] we suggest to call this phase β-hexagonal ammonium tungsten bronze (β-HATB), β-$(NH_4)_xWO_{3-y}$ in order to distinguish it from the well-known α-hexagonal ammonium tungsten bronze. When studying α- and β-HATB at the same time, it is necessary to make a difference between them with greek letters, but in other cases α-HATB can be called simply HATB, since it is the most common hexagonal ammonium tungsten bronze.

We checked the two ICDD cards assigned to β-HATB by comparing them with the simulated powder XRD pattern of this phase. Volkov et al. [37] detected one more reflection ($d = 0.2864$ nm) compared to us, however, this extra reflection did not fit into the simulated pattern. We suppose that this reflection might be the result of some contamination. This is supported also by that even Volkov et al. could not index this reflection. We think that the phase Neugebauer et al. [35] observed was also this hexagonal phase. They observed two reflections around 48° instead of one, and three reflections around 57° instead of one. However, their extra reflections did not even fit into a tetragonal structure. The reflections of β-HATB around 48° and 57° might have been not sharp enough by Neugebauer et al. (they were recording the XRD patterns by a Guinier camera on a photofilm, which they read by using a photometer), and thus they could have deconvoluted these peaks into more reflections than they were in real.

Efforts were made to determine the atomic coordinates of β-HATB by Rietveld analysis. For the analysis a starting structure was needed. There was a chance that the structure β-HATB was similar to that of α-HATB or h-WO_3 (all structures were hexagonal with similar lattice parameters), and for both phases there were already published atomic coordinates. Therefore, we tried to calculate the atomic coordinates of β-HATB using the previously published structures of α-HATB [42] and h-WO_3 [43] as initial structures. The extinction rules allowed several space groups for the powder XRD of β-HATB. The starting structures of α-HATB or h-WO_3 were refined in the most propable space groups (P6/m, P6/mmm, P6/mcm) from the several allowed ones, and several parameters were varied. However, it turned out that the structure of β-HATB did not resemble to any of our initial structural models, and Rietveld results did not converge to a certain structure in any of the studied cases,

Table 2 Powder XRD data of β-HATB, $(NH_4)_{0.001}WO_{2.79}$

Nr.	*d*/nm	2θ/°	I/I_0/%	*hkl*
1	0.3784	23.511	100.0	002
2	0.3163	28.213	30.0	200
3	0.2427	37.043	25.0	202
4	0.1892	48.092	20.0	004
5	0.1624	56.692	15.0	204
6	0.1261	75.353	5.0	006
7	0.1172	82.296	3.0	206

thus atomic coordinates of β-HATB could not be determined. In conclusion, as there was no basic structural model available, the present data were not enough for a proper Rietveld analysis of β-HATB. Nevertheless, with our results it was possible to decide that β-HATB had hexagonal unit cell, which had been disputed for 50 years in the literature.

A solution might be to determine the exact structure of β-HATB, if it could be obtained in single crystals. This could be achieved if single crystals of α-HATB were available, as the morphology does not change going from α- to β-HATB. However, this requires a novel wet chemical preparation route, since the present route to get α-HATB (thermal reduction of ammonium paratungstate tetrahydrate (APT), $(NH_4)_{10}[H_2W_{12}O_{42}]\cdot 4H_2O$ [31, 33]) yields only nanocrystals.

Besides its structure, we also investigated the morphology and composition of β-HATB. Note that neither Neugebauer et al., nor Volkov et al. presented a complete chemical and morphological analysis of this phase. SEM study revealed that the morphology of β-HATB was similar to that of reduced h-WO_3 and α-HATB (Fig. 6), as β-HATB was also built up by 50–100 nm aggregated nanoparticles. Therefore, the change in crystalline structure between reduced h-WO_3 and β-HATB did not induce significant morphology changes.

XPS showed that β-HATB was even further reduced than reduced h-WO_3 and α-HATB (Fig. 3; Table 1). The highly reduced state of the sample was supported by its dark blue colour, and also by the Raman spectrum (Fig. 4), as Raman peaks became even broader than by reduced h-WO_3. Raman also revealed a change in the bonds of β-HATB compared to reduced h-WO_3. In small amounts NH_4^+ was still present in β-HATB as detected by ^{1}H-MAS NMR (Fig. 5) and TG/DTA-MS (Fig. 1).

The composition of β-HATB was determined by combining the results of different measurements. The W/O ratio was calculated by integrating the W4f and O1s region in the XPS spectrum. The amount of residual NH_4^+ was determined by ^{1}H-MAS NMR. As a result, the formula of β-HATB sample was determined to be $(NH_4)_{0.001}WO_{2.79}$. The formula suggests that β-HATB is basically a reduced tungsten oxide, and the tiny NH_4^+ content might have the role of increasing the stability of the structure—similar as by h-WO_3 [33].

Reduction of β-HATB

Between 650 and 800 °C H_2O and small amounts of NH_3 were released, while β-HATB started to decompose into γ-tungsten oxide, $WO_{2.72}/W_{18}O_{49}$ (ICDD 05-0392, 36-0102) and δ-tungsten oxide, WO_2 (ICDD 32-1393). Between 750 and 800 °C a previously unexplained exothermic DTA peak was detected (Fig. 1), whose explanation we give below. During the thermal reduction of APT we observed a similar exothermic heat effect around 750 °C, which we assigned to the formation and crystallization heat of $WO_{2.72}/W_{18}O_{49}$ [30]. Here the situation was the same as by APT. At first look, the exothermic heat effect between 750 and 800 °C might be related to the appearance of either $WO_{2.72}/W_{18}O_{49}$ or WO_2, since the amount of both of these phases increased between 750 and 800 °C. But in the seventh decomposition step (800–900 °C), where practically only WO_2 formed, there was no sharp heat effect, so the exothermic heat effect between 750 and 800 °C could not belong to the formation of WO_2. Thus, this exothermic heat effect was explained with the formation and crystallization heat of $WO_{2.72}/W_{18}O_{49}$.

Finally in the seventh decomposition step (from 800 °C) H_2O was released as reduction product of tungsten oxides without any sharp heat effect. The intermediate at 900 °C consisted of WO_2 with traces of α-tungsten, W (ICDD 04-0806) and $WO_{2.72}/W_{18}O_{49}$.

Conclusions

The formation and structure of all three kinds of ammonium tungsten bronzes, $(NH_4)_{0.33-x}WO_{3-y}$ was studied. When α-hexagonal ammonium tungsten bronze (α-HATB), $(NH_4)_{0.08}(NH_3)_{0.04}(H_2O)_{0.09}WO_{2.93}$, was thermally reduced in 10% H_2/Ar, NH_3 left the solid structure between 250 and 650 °C in three overlapping steps. The release of NH_3 below 400 °C was unexpected (because α-HATB was produced by heating APT at 400 °C in H_2). It could be rationalized either by cracking of α-HATB after its preparation at 400 °C, or by rearrangement of NH_4^+ ions and NH_3 molecules in a solid state chemical equilibrium reaction. The evolution of NH_3 in three overlapping steps was explained by that NH_3 (originated from the NH_4^+ and NH_3 content of α-HATB) came from three different positions of the solid structure.

Around 550 °C the second type of hexagonal ammonium tungsten bronzes formed, whose structure was similar to α-HATB, but the hexagonal channels were almost completely empty. To be consistent with literature, this phase was called reduced hexagonal WO_3. By analysing the XRD patterns and the composition of α-HATB and various h-WO_3 samples, we concluded that the oxidation state of W atoms influenced at least as much the cell parameters of α-HATB and h-WO_3, as the occupancy of the hexagonal channels. This is significant, since previously only packing of the hexagonal channels was considered to be decisive on the cell parameters of h-WO_3 and α-HATB (and in general also on the cell parameters of hexagonal tungsten bronzes).

When reduced h-WO_3 was heated further, the metastable hexagonal tungsten oxide framework collapsed in an

exothermic reaction and transformed into the third type of ammonium tungsten bronzes. It was disputed whether this latter phase had tetragonal (ICDD 15-0217) or hexagonal (ICDD 42-0451) structure. The fact that we could prepare this phase in a pure form allowed us to decide this question. By obtaining precise powder XRD data, we concluded that this phase, β-hexagonal ammonium tungsten bronze (β-HATB), had hexagonal structure. The composition of β-HATB was determined more precisely than earlier, and the following formula was obtained: $(NH_4)_{0.001}WO_{2.79}$.

When β-HATB was reduced further between 650 and 900 °C, the formation of reduced tungsten oxides ($WO_{2.72}/W_{18}O_{49}$, WO_2), and to a small degree that of tungsten metal was confirmed. We observed that the formation of γ-tungsten oxide, $WO_{2.72}/W_{18}O_{49}$ was an exothermic reaction.

Recently it was found that the partial reduction of ammonium paratungstate (APT), $(NH_4)_{10}[H_2W_{12}O_{42}]\cdot 4H_2O$ yields a very high quality, pure and nanosize α-HATB [31]. In this study it was shown that further reduction of α-HATB is a fast and facile way to prepare the other two kinds of hexagonal ammonium tungsten bronzes in nanosize and pure form for various applications.

Acknowledgements I. M. S. thanks for an Aschner Lipót scholarship of GE Hungary ZRt., GE Consumer and Industrial–Lighting. A diffractometer purchase grant from the Agency for Research Fund Management (KPI-EU-GVOP-3.2.1.-2004-04-0224/3.0 KMA) and a Hungarian GVOP-3.2.1.-2004-04-0210/3.0 grant are gratefully acknowledged.

References

1. Pedrosa AMG, Souza MJB, Marinkovic BA, Melo DMA. Structure and properties of bifunctional catalysts based on zirconia modified by tungsten oxide obtained by polymeric precursor method. Appl Catal A. 2008;342:56–62.
2. Irie H, Miura S, Kamiya K, Hashimoto K. Efficient visible light-sensitive photocatalysts: grafting Cu(II) ions onto TiO_2 and WO_3 photocatalysts. Chem Phys Lett. 2008;457:202–5.
3. Huang T, Lin X, Xing J, Wang W, Shan Z, Huang F. Photocatalytic activities of hetero-junction semiconductors $WO_3/SrNb_2O_6$. Mater Sci Eng B. 2007;141:49–54.
4. Yang J, Li Y, Huang Y, Liang J, Shen PK. Dynamic conducting effect of WO_3/PFSA membranes on the performance of proton exchange membrane fuel cells. J Power Sources. 2008;177:56–60.
5. Dillon AC, Mahan AH, Deshpande R, Parilla PA, Jones KM, Lee SH. Metal oxide nano-particles for improved electrochromic and lithium-ion battery technologies. Thin Solid Films. 2008;518:794–7.
6. Higashimoto S, Shishido T, Ohno Y, Azuma M, Takahashi M, Anpo M. Photocharge-discharge behaviors of hybrid WO_3/TiO_2 film electrodes: conversion, storage of electrons, and the effect of the WO_3 structure on rechargeability. J Electrochem Soc. 2007;154:F48–54.
7. Suda Y, Kawasaki H, Ahshima T, Yagyuu Y. Characteristics of tungsten oxide thin films prepared on the flexible substrates using pulsed laser deposition. Thin Solid Films. 2008;516:4397–401.
8. Gubbala S, Thangala J, Sunkara MK. Nanowire based electrochromic devices. Sol Energy Mater Sol C. 2008;91:813–20.
9. Todorovski T, Najdowski M. The solution growth route and characterization of electrochromic tungsten oxide thin films. Mater Res Bull. 2007;42:2025–31.
10. Grandqvist CG. Handbook of inorganic electrochromic materials. Amsterdam: Elsevier; 1995.
11. Wang S, Feng X, Yao J, Jiang L. Controlling wettability and photochromism in a dual-responsive tungsten oxide film. Angew Chem Int Ed Engl. 2006;45:1264–7.
12. He Y, Wu Z, Fu L, Li C, Miao Y, Cao L, et al. Photochromism and size effect ofWO_3 and WO_3-TiO_2 aqueous sol. Chem Mater. 2003;15:4039–45.
13. Chen H, Xu N, Deng S, Lu D, Li Z, Zhou J, et al. Gasochromic effect and relative mechanism of WO_3 nanowire films. Nanotechnology. 2007;18:205701 (6 pp).
14. Lu DY, Chen J, Chen HJ, Gong L, Deng SZ, Xu NS. Raman study of thermochromic phase transition in tungsten trioxide nanowires. Appl Phys Lett. 2007;90:041919 (3 pp).
15. Durrani SMA, Khawaja EE, Salim MA, Al-Kuhaili MF, Al-Shukri AM. Effect of preparation conditions on the optical and thermochromic properties of thin films of tungsten oxide. Sol Energy Mater Sol Cell. 2002;71:313–25.
16. Balázsi C, Wang L, Zayim EO, Szilágyi IM, Sedlackova K, Pfeifer J, et al. Nanosize hexagonal tungsten oxide for gas sensing applications. J Eur Ceram Soc. 2008;28:913–7.
17. Siciliano T, Tepore A, Micocci G, Serra A, Manno D, Filippo E. WO_3 gas sensors prepared by thermal oxidization of tungsten. Sens Actuators B Chem. 2008;133:321–6.
18. Kanan SM, Waghe A, Jensen BL, Tripp CP. WO_3 based sensors to selectively detect DMMP in the presence of alcohols. Talanta. 2007;72:401–7.
19. Huelser TP, Lorke A, Ifeacho P, Wiggers H, Shulz C. Core and grain boundary sensitivity of tungsten-oxide sensor devices by molecular beam assisted particle deposition. J Appl Phys. 2007;102:124305 (7 pp).
20. Lassner E, Schubert W-D. Tungsten. Properties, chemistry, technology of the element, alloys, and chemical compounds. New York: Kluwer Academic/Plenum Publishers; 1999.
21. Bartha L, Lassner E, Schubert W-D, Lux B, editors. Special issue on the chemistry of non-sag tungsten. Int J Refract Met Hard Mater 1995;13:1–164.
22. Lunk H-J, Ziemer B, Salmen M, Heidemann D. What is behind 'tungsten blue oxides'? Int J Refract Met Hard Mater. 1993/1994;12:17–26.
23. Lunk H-J, Salmen M, Heidemann D. Solid state ^{1}H NMR studies of different tungsten blue oxides and related substances. Int J Refract Met Hard Mater. 1998;16:23–30.
24. Kiss BA, Rom Berendné G, Gyarmathy G, Kutasi Feketéné Z. Ammónium-volfrámoxidbronz porkohászati alapanyag reduktív termikus bomlása. Magyar Kémiai Folyóirat (Hung). 1987;93:97–106.
25. Bartha L, Gyarmati G, Kiss BA, Németh T, Salamon A, Szalay T. Complex studies on intermedier decomposition products of amonium paratungstate. Acta Chim Acad Sci Hung. 1979;101:127–38.
26. Huao L, Zhao H, Mauvy F, Fourcade S, Labrugere C, Pouchard M, et al. Synthesis and mixed conductivity of ammonium tungsten bronze with tunneling structures. Solid State Sci. 2004;6:679–88.
27. Gier TE, Pease DC, Sleight AW, Bither TA. New lithium, ammonium, and tin hexagonal tungsten bronzes prepared hydrothermally. Inorg Chem. 1968;7:1646–7.

28. Michailovski A, Krumeich F, Patzke GR. Hierachical growth of mixed ammonium molybdenum/tungsten bronze nanorods. Chem Mater. 2004;16:1433–40.
29. Zhan JH, Yang XG, Xie Y, Li BF, Qain YT, Jia YB. A solvothermal route for the synthesis of ammonium tungsten bronze. Solid State Ionics. 1999;126:373–7.
30. Szilágyi IM, Madarász J, Hange F, Pokol G. Partial thermal reduction of ammonium paratungstate tetrahydrate. J Therm Anal Calorim. 2007;88:139–44.
31. Szilágyi IM, Hange F, Madarász J, Pokol G. In situ HT-XRD study on the formation of hexagonal ammonium tungsten bronze by partial reduction of ammonium paratungstate tetrahydrate. Eur J Inorg Chem. 2006;17:3413–8.
32. Szilágyi IM, Madarász J, Hange F, Pokol G. On-line evolved gas analyses (EGA by TG-FTIR and TG/DTA-MS) and solid state (FTIR, XRD) studies on thermal decomposition and partial reduction of ammonium paratungstate tetrahydrate. Solid State Ionics. 2004;172:583–6.
33. Szilágyi IM, Madarász J, Király P, Tárkányi G, Tóth AL, Szabó A, et al. Stability and controlled composition of hexagonal WO_3. Chem Mater. 2008;20:4116–25.
34. Mészáros M, Neugebauer J, Hange F. Processes of reductive decomposition of APT above 400°C; Transformation of APT → KTB → β-W in the presence of K. High Temp Mater Proc. 1996;15:111–5.
35. Neugebauer J, Hegedűs AJ, Millner T. Über die Reduktion des Ammoniumwolframates und Wolframtrioxyds mittels Ammoniak. Z Anorg Allg Chem. 1959;302:50–9.
36. Szilágyi IM, Madarász J, Pokol G, Hange F, Szalontai G, Varga-Josepovits K, et al. The effect of K^+ ion doping on the structure and thermal reduction of hexagonal ammonium tungsten bronze. J Therm Anal Calorim 2009; doi:10.1007/s10973-008-9752-1.
37. Volkov VL. Synthesis and investigation of ammonium tungsten bronze. (Engl transl). Izv Akad Nauk SSSR Neorg Mater (Russ). 1990;26:125–9.
38. Madarász J, Szilágyi IM, Hange F, Pokol G. Comparative evolved gas analyses (TG-FTIR, TG/DTA-MS) and solid state (FTIR, XRD) studies on thermal decomposition of ammonium paratungstate tetrahydrate (APT) in air. Anal Appl Pyrolysis. 2004;72:197–201.
39. Cory DG, Ritchey WM. Suppression of signals from the probe in Bloch decay spectra. J Magn Reson. 1988;80:128–32.
40. Ramana CV, Utsunomiya S, Ewing RC, Julien CM, Becker U. Structural stability and phase transitions in WO_3 f. J Phys Chem B. 2006;110:10430–5.
41. Szilágyi IM, Pfeifer J, Balázsi C, Tóth AL, Varga-Josepovits K, Madarász J, et al. Thermal stability of hexagonal tungsten trioxide. J Therm Anal Calorim. 2008;98:499–505.
42. Dickens PG, Halliwell AC, Murphy DJ, Wittingham MS. Preparation and characterization of a hexagonal ammonium tungsten bronze phase $(NH_4)_xWO_3$. Trans Farad Soc. 1971;67:794–800.
43. Oi J, Kishimoto A, Kudo T, Hiratani M. Hexagonal tungsten trioxide obtained from peroxo-polytungstate and reversible lithium electro-intercalation into its framework. J Solid State Chem. 1992;96:13–9.